THE JOURNAL OF PHYSICAL CHEMISTRY Letters

Letter

Cite This: J. Phys. Chem. Lett. 2018, 9, 6262−6268

pubs.acs.org/JPCL

Mechanism of Exact Transition between Cationic and Anionic Redox Activities in Cathode Material Li_2FeSiO_4

Jiaxin Zheng,[†,#] Gaofeng Teng,[†,#] Jinlong Yang,[†,#] Ming Xu,[†] Qiushi Yao,[‡] Zengqing Zhuo,[†,§] Wanli Yang,[§] Qihang Liu,*[,‡] and Feng Pan*[,†]

[†]School of Advanced Materials, Peking University, Shenzhen Graduate School, Shenzhen 518055, China

[‡]Shenzhen Institute for Quantum Science and Engineering and Department of Physics, Southern University of Science and Technology, Shenzhen 518055, China

[§]Advanced Light Source, Lawrence Berkeley National Laboratory, Berkeley, California 94720, United States

Supporting Information

ABSTRACT: The discovery of anion redox activity is promising for boosting the capacity of lithium ion battery (LIB) cathodes. However, fundamental understanding of the mechanisms that trigger the anionic redox is still lacking. Here, using hybrid density functional study combined with experimental soft X-ray absorption spectroscopy (sXAS) measurements, we unambiguously proved that $Li_{(2-x)}FeSiO_4$ performs sequent cationic and anionic redox activity through delithiation. Specifically, Fe^{2+} is oxidized to Fe^{3+} during the first Li ion extraction per formula unit (f.u.), while the second Li ion extraction triggered the oxygen redox exclusively. Cationic and anionic redox result in electron and hole polaron states, respectively, explaining the poor conductivity of $Li_{(2-x)}FeSiO_4$ noted by previous experiments. In contrast, other cathode materials in this family exhibit diversity of the redox process. Li_2MnSiO_4 shows double cationic redox (Mn^{2+}−Mn^{4+}) during the whole delithiation, while Li_2CoSiO_4 shows simultaneous cationic and anionic redox. The present finding not only provides new insights into the oxygen redox activity in polyanionic compounds for rechargeable batteries but also sheds light on the future design of high-capacity rechargeable batteries.

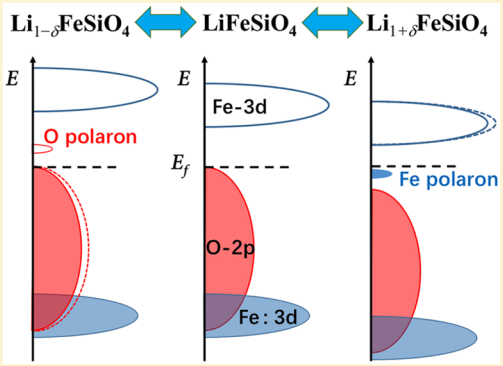

Charge compensation of transition metals (TMs) in TM-based compounds when the total charge of the compound is altered (e.g., through oxidation/reduction, carrier injection, chemical doping) is a fundamental and intriguing topic in both physics and chemistry.[1,2] Classic inorganic chemistry tacitly assumes that most of the changes of the total charge are accommodated by a change in the charge of the TM ion.[3,4] Typically, for rechargeable lithium ion battery (LIB) cathode materials, TM ions were regarded as the sole sources of electrochemical activity in an intercalation cathode to provide charge-compensating electrons after Li ion extraction.[5−9] As a result, the theoretical capacity of these oxides has been limited by the number of electrons offered by the TM redox reaction and its relatively high atomic weight.

Until recently, this scenario was challenged by the discovery of anionic redox activity in Li-rich layered TM oxides.[10−19] Additionally, the discovery of anionic redox activity has been extended to other kinds of cathode materials beyond Li-rich layered TM oxides, such as nonlayered TM oxides[20,21] and metal−organic compounds.[22] Anionic reduction not only extends our understanding of the charge compensation process during delithiation in cathodes but also raises the opportunity to boost the capacity and energy density of LIBs by combining both cationic and anionic redox processes within the same material.[14,23,24]

However, such staggering capacities suffer from capacity fade with cycling,[25] which is mainly due to the irreversible loss of lattice oxygen during the anionic redox process.[15,19,26] Thus, clarifying the specific redox mechanism and fundamental understanding of the local structure and electronic state evolutions during the anionic redox process become crucial for both experimentalists and theorists. In general, three types of redox processes are revealed in the reported cathode materials with anionic redox, including (1) cationic redox first and anionic redox next, such as in layered NMC,[15,27,28] (2) simultaneous cationic and anionic redox, such as in Li_5FeO_4,[20] and (3) anionic redox only, such as in Li_2MnO_3.[29−31] Here, we focus on a series of silicate cathode materials $Li_{(2-x)}TMSiO_4$ (TM = Mn, Fe, Co, and Ni), for which the mechanism of redox activity is still under debate.[32−39] Using hybrid density functional study combined with the modern perspective of doping and experimental soft X-ray absorption spectroscopy

Received: September 5, 2018
Accepted: October 16, 2018
Published: October 16, 2018

DOI: 10.1021/acs.jpclett.8b02725
J. Phys. Chem. Lett. 2018, 9, 6262−6268

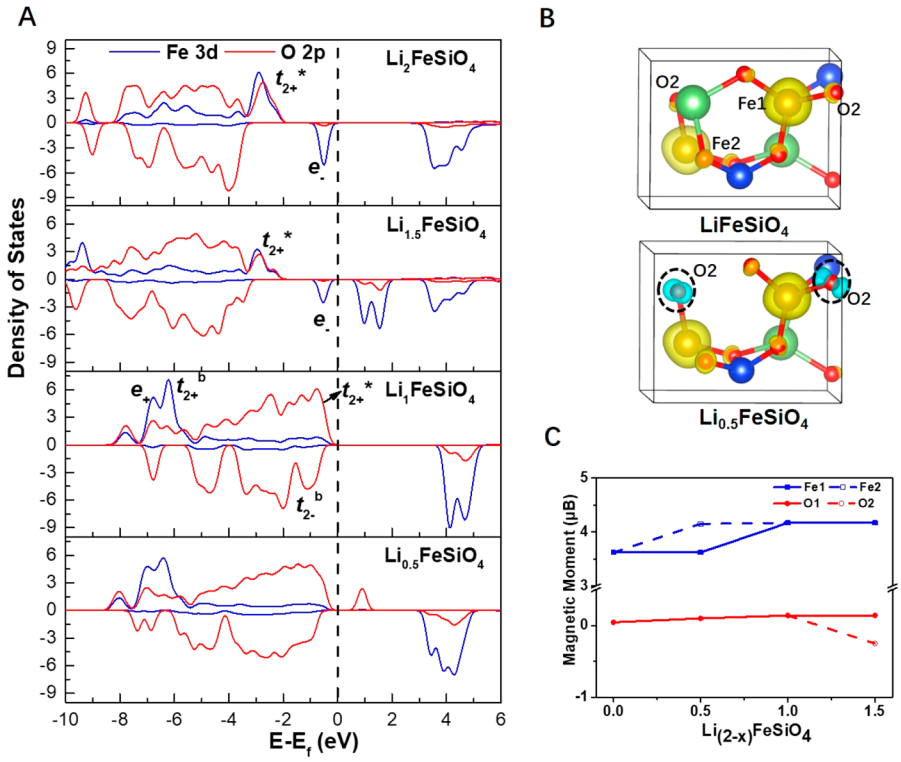

Figure 1. HSE calculated electronic structures for $Li_{(2-x)}FeSiO_4$ during delithiation. (A) Projected density of states (PDOS) of Fe-3d and O-2p states in $Li_{(2-x)}FeSiO_4$ (x = 0, 0.5, 1.0, and 1.5). (B) Isosurface of the spin density in the unit cell of partially delithiated $Li_{(2-x)}FeSiO_4$ (x = 1.0 and 1.5). Green, Li; red, O; dark blue, Si; brown, Fe. The isovalues for the isosurfaces of the spin densities were 0.05 e $Å^{-3}$ for all cases. (C) Calculated magnetic moment of Fe and O in $Li_{(2-x)}FeSiO_4$ at different delithiation states. O1 and O2 denote two kinds of O ions with different variations of the magnetic moment in $Li_{(2-x)}FeSiO_4$. O2 are denoted in (B), and all of the remaining unidentified O ions in (B) are O1.

(sXAS) measurements, we proved that $Li_{(2-x)}FeSiO_4$ ($0 < x < 2$) performs sequent cation and anionic redox activity upon delithiation. During delithiation, our results demonstrated that Fe^{2+} ions change to Fe^{3+} until a critical Li concentration $x = 1$, while further Li extraction triggers oxygen redox instead of cation oxidation. In order to uncover the physical origin of the exact transition point ($x = 1$) of cationic/anionic redox, we then focused on dilute lithiation and delithiation behaviors of $LiFeSiO_4$ and found that both of lithiation and delithiation processes result in a polaronic state, but with cationic and anionic character, respectively. In contrast to the previous reported oxygen clustering during oxygen redox in Li-rich layered TM oxides, the oxygen polaron in $Li_{(2-x)}FeSiO_4$ is localized on a single O ion, which avoids peroxo-like O−O bond formation to prevent the lattice O loss. Moreover, we found that not all of the polyoxyanion $Li_{(2-x)}TMSiO_4$ exhibit such polaronic oxygen redox activity after more than one Li ion is extracted but show a strong dependence on the 3d occupation numbers of TM elements.

In the polyoxyanion-type intercalation $Li_{(2-x)}FeSiO_4$ structures, each iron, lithium, and silicon atom is coordinated by four oxygen atoms, while the FeO_4 tetrahedra are cross-linked by silicate groups (Figure S1). The electrochemical performance of Li_2FeSiO_4 is discussed in Supporting Information Note 1. The first discharge specific capacity is 305 mAh/g, corresponding to 1.86 Li-storages per Li_2FeSiO_4 unit with oxygen redox occurring, close to the previously reported performance of Li_2FeSiO_4 nanocrystals.[34] To reveal the underlying mechanism of the redox process during delithiation, we perform DFT calculations to revisit different delithiation stages of $Li_{(2-x)}FeSiO_4$ and compare the results with our sXAS measurements. The general challenge of standard exchange−correlation functionals in DFT is the notorious self-interaction error (SIE). Therefore, previous DFT studies even predicted a metallic state for $Li_{(2-x)}FeSiO_4$ during delithiation,[32,40] in sharp contrast to the semiconducting phase as reported by experiments.[41,42]

Sequent Cation and Anion Redox in $Li_{(2-x)}FeSiO_4$. We first apply a hybrid functional in the form of Heyd−Scuseria−Ernzerhof (HSE06)[43] to correct the SIE. The evolution of the density of states for the unit cell ($Li_4Fe_2Si_2O_8$) of partially delithiated $Li_{(2-x)}FeSiO_4$ (x = 0, 0.5, 1.0, and 1.5) is shown in Figure 1A (the corresponding crystal structures is shown in Figure S3). It is found that when x goes from 0 to 1.5, the band gap E_g changes from 2.91 ($x = 0$) to 3.60 and 0.57 eV for $x = 1$ and 1.5, respectively, consistent with the semiconducting phase as reported by experiments.[41,42] Moreover, our results naturally explain that $Li_{(2-x)}FeSiO_4$ always keeps a poor electronic conductivity and rate capability during electrochemical cycling.[44] From the top three panels of Figure 1A, we can see that the Fe-3d peak right below the Fermi level is gradually shifted upward after the first Li extraction per f.u., indicating the redox couple of Fe^{2+}/Fe^{3+}. However, the second Li ion extraction shifts valence states with pure O-2p character across the Fermi level (Figure 1A, bottom panel), indicating that instead of Fe^{3+}/Fe^{4+} it is an O anion playing an active role. Interestingly, the upward shifted O-2p states form a localized, polaron-like hole state inside of the band gap of $LiFeSiO_4$. Such a hole-localized state is confirmed by the isosurface of the spin density of partially delithiated $Li_{(2-x)}FeSiO_4$ (x = 1 and 1.5), as shown in Figure 1B. We observe large spin density from two oxygen ions with the shape of an isolated O-2p

DOI: 10.1021/acs.jpclett.8b02725
J. Phys. Chem. Lett. 2018, 9, 6262−6268

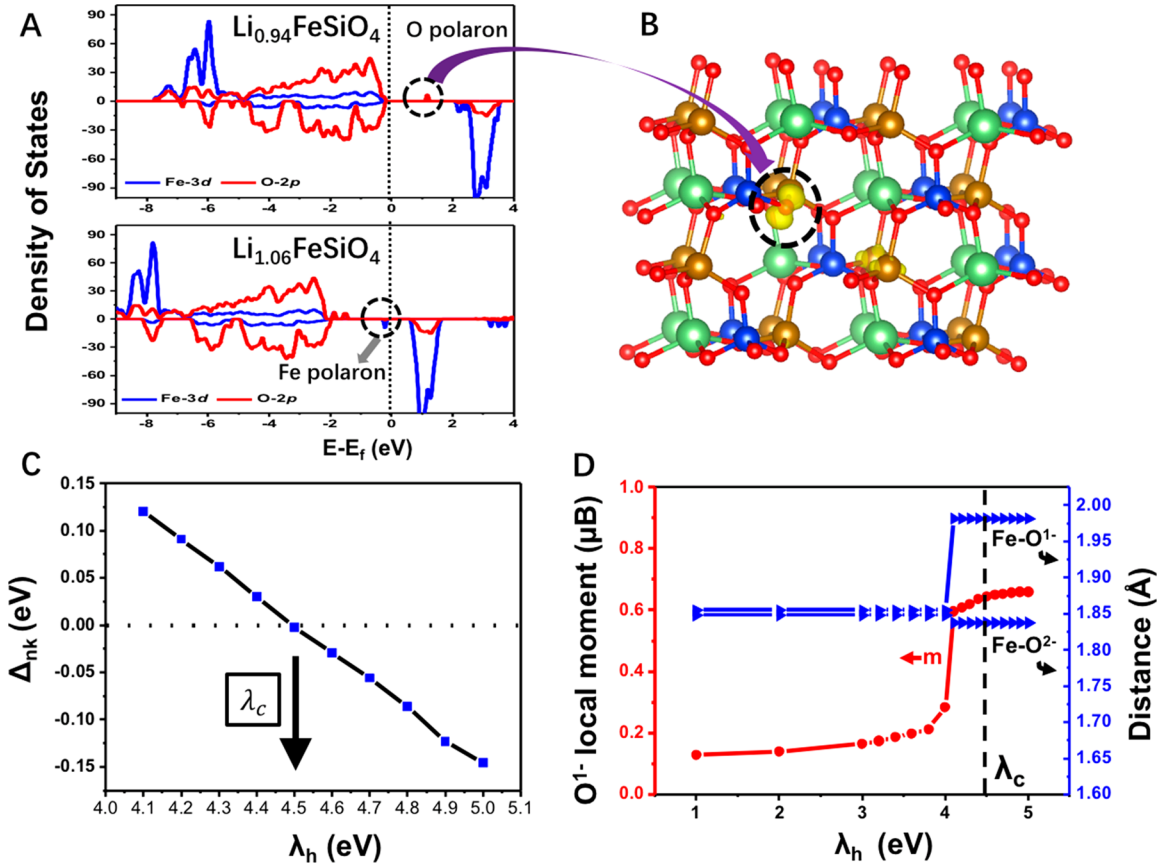

Figure 2. Cation/anion transition at the critical point $x = 1$. (A) PDOS of Fe-3d and O-2p states in $Li_{15}Fe_{16}Si_{16}O_{64}$ (delithiation, top panel) and $Li_{17}Fe_{16}Si_{16}O_{64}$ (lithiation, bottom panel). (B) Isosurface of the charge density of the O polaron state in the cell of $Li_{15}Fe_{16}Si_{16}O_{64}$, showing localization on a single O ion. (C) Non-Koopmans energy Δ_{nk} (see eq 1) as a function of the hole-state potential strength λ_h (see eq 2). (D) Structural and magnetic properties of the O^- in $Li_{15}Fe_{16}Si_{16}O_{64}$ as a function of the hole-state potential strength λ_h. The polaronic state is stable above a value $\lambda_h > 4.0$ eV, while the critical value λ_c that fulfills the generalized Koopmans theory is marked by the dashed line. *m*: local magnetic moment of O^-.

orbital for $Li_{0.5}FeSiO_4$, indicating that this polaron state is localized on two O ions belonging to one SiO_4 tetrahedron. The calculated magnetic moments of Fe and O in partially delithiated $Li_{(2-x)}FeSiO_4$ (Figure 1C) also support the whole redox process analyzed above. From Li_2FeSiO_4 to $LiFeSiO_4$, the magnetic moments of the two Fe cations change from 3.61 μB (Fe^{2+}, $e_g^3t_{2g}^3$) to 4.17 μB (Fe^{3+}, $e_g^2t_{2g}^3$) by sequence. For the further delithiation (from $x = 1$ to 1.5), the magnetic moments of Fe ions remain nearly unchanged, while the magnetic moments of two O ions (unchanged from Li_2FeSiO_4 to $LiFeSiO_4$) start to change to -0.25 μB in $Li_{0.5}FeSiO_4$. The structural response to the creation of hole polarons is discussed in Supporting Information Note 2. We find that two adjacent O ions form localization centers of the isolated state for $Li_{0.5}FeSiO_4$, indicating a $2O^{2-}/(O_2)^{3-}$ process, which is similar to the peroxo-like oxygen redox process in layered TM oxides.[11,16−19,25] To further confirm the above theoretical calculations, the Fe L-edge and O K-edge sXAS of samples Li_2FeSiO_4, Li_1FeSiO_4, and $Li_{0.15}FeSiO_4$ are tested, as shown in Figure S5A,B, respectively. Our sXAS results provide consistent evidence for the physical picture suggested by our theoretical calculations. (see Supporting Information Note 3 for details).

Cation/Anion Transition at the Critical Point x = 1. A general discussion of the origin of anionic redox activity in $Li_{(2-x)}FeSiO_4$ can be found in Supporting Information Note 4. In the following, to get a microscopic picture of how the switch between cation and anion redox is triggered at the transition point $x = 1$ for $Li_{(2-x)}FeSiO_4$, we focused on lithiation and delithiation behaviors of $LiFeSiO_4$ at a small concentration, which corresponds to a doping perspective. The challenge of such prediction of dilute doping lies in that especially for delithiation the localized hole states are often incorrectly described in standard DFT exchange−correlation functionals as rather delocalized states that spread over all oxygen ligands.[45−47] Such "delocalization error"[48] originates from the convex bowing of the total energy $E(N)$ with respect to electron occupation number N. Indeed, a perfect correction is required to fulfill the so-called generalized Koopmans condition

$$\Delta_{nk} = E(N+1) - E(N) + \mathrm{eig}(N) = 0 \quad (1)$$

where $E(N+1) - E(N)$ denotes the total energy cost to add an electron from the hole-doped system and $\mathrm{eig}(N)$ is the single-particle energy of the lowest unoccupied state in the electron-doped system. Here we use the Lany−Zunger approach[49] to restore the generalized Koopmans condition (see the Supporting Information for details). Basically, we introduce an onsite potential implemented as the combination of DFT+U and nonlocal external potentials[50] to certain atomic orbitals. For hole doping, the corresponding electron state potential is given by

DOI: 10.1021/acs.jpclett.8b02725
J. Phys. Chem. Lett. 2018, 9, 6262−6268

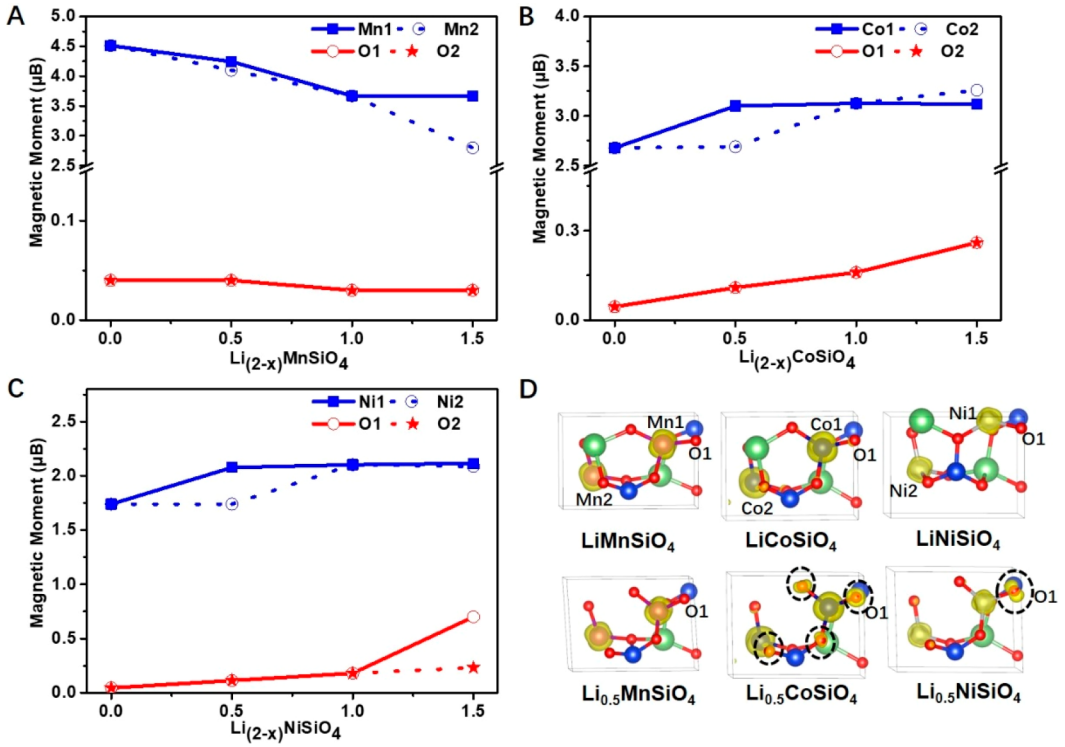

Figure 3. Redox activity in other $Li_{(2-x)}TMSiO_4$ compounds. (A–C) Calculated magnetic moment of TM and O in $Li_{(2-x)}TMSiO_4$ (TM = Mn, Co, and Ni) at different delithiation states. O1 are denoted in (D), and all of the remaining unidentified O ions in (D) are O2. (D) Isosurface of the spin density in the unit cell of partially delithiated $Li_{(2-x)}TMSiO_4$ (x = 1.0 and 0.5). Green, Li; red, O; dark blue, Si; purple, Mn; light blue, Co; silver, Ni.

$$V_h = \lambda_h(1 - n_{m,\sigma}/n_{host}) \quad (2)$$

where $n_{m,\sigma}$ and n_{host} denote the occupation of the m sublevel of spin σ and the occupation of the host material without doping, respectively. We determine n_{host} in eq 2 to be 0.595 from the partial charge of the O-p orbitals of the occupied states. The parameter λ_h is tuned to perfectly fulfill the linearity of $E(N)$, i.e., the generalized Koopmans condition eq 1.

Starting from the cation/anion transition point (x = 1), we use a 2 × 2 × 2 supercell (16 Li atoms per cell) of $LiFeSiO_4$ and remove or add one Li atom to achieve a relatively low carrier doping concentration (~6%). By removing one Li atom, the projected density of states (PDOS) of $Li_{0.94}FeSiO_4$ (Figure 2A, top panel) exhibits a localized O acceptor state inside of the fundamental band gap between the Fe-like Hubbard band and O-like charge-transfer band, similar to $Li_{0.5}FeSiO_4$ (Figure 1A). Note that here we choose λ_h to be the critical value λ_c = 4.5 eV, at which point the generalized Koopmans condition eq 1 is exactly fulfilled, i.e., Δ_{nk} = 0 (Figure 2C). However, the charge density of the localized state (Figure 2B) shows that the small oxygen polaron in $Li_{0.94}FeSiO_4$ is localized on a single O ion, rather than an $(O_2)^{3-}$ cluster for high delithiation concentrations. Such a scenario of a single-O polaron is further verified by the structural and magnetic properties around the Li vacancy. As shown in Figure 2D, when the hole-state potential strength exceeds a critical value of 4.0 eV, a breaking of the tetrahedral symmetry occurs, evidenced by the fact that one Fe–O^- bond is apparently elongated compared with the other three Fe–O^{2-} bonds and so are the Si–O bonds. In contrast, a standard DFT +U calculation (λ_h = 0) or small λ_h predicts a high-symmetry extended acceptor state with an equal amplitude of all Fe–O and Si–O bonds. The polaronic state also suggests the emergence of a local magnetic moment at the O^- ion that traps the hole. Because our λ_h that fulfills eq 1 (4.5 eV) is higher than the transition value (4.0 eV), the stabilized single-O polaronic state is predicted to be the physical reality in the delithiation process with low concentration. This means that in $LiFeSiO_4$ delithiation starts by forming a single-O^- polaron, while the O clusters begin to form when an amount of elongated Fe–O bonds is close enough at a relatively high concentration (e.g., x = 1.5).

On the other hand, adding one Li to $LiFeSiO_4$ (leading to $Li_{1.06}FeSiO_4$) exhibits an electron polaron state dominated by Fe-3d orbitals, as shown in Figure 2A (bottom panel). As a result, associated with this lithiation process, an Fe^{3+} ion is reduced to Fe^{2+}, corresponding to traditional cation redox activity. Note that we did not apply any onsite potential on the donor state here because, similar to other Fe^{3+} system such as Fe_2O_3, DFT+U already satisfies the generalized Koopmans condition in good approximation.[51] Overall, by a dilute doping approach, we observe exact cation/anion redox transition at $LiFeSiO_4$ (x = 1), with electron/hole single-polaron formation for the cation/anion redox process.

Redox Activity in Other $Li_{(2-x)}TMSiO_4$ Compounds. We next consider other $Li_{(2-x)}TMSiO_4$ (TM = Mn, Co, and Ni) materials[32,52−56] to see whether the existence of oxygen redox activity is universal among these polyanionic materials. For $Li_{(2-x)}MnSiO_4$, PDOS plots show that upon delithiation from x = 0 up to x = 1.5 the cation valence $Mn^{2+} \rightarrow Mn^{3+} \rightarrow Mn^{4+}$ accounts for the redox activity (Figure S8). It should be noted that there is also a small portion of oxygen redox activity accompanied by the main Mn redox. The calculated magnetic moments of Mn in partially delithiated $Li_{(2-x)}MnSiO_4$ also

DOI: 10.1021/acs.jpclett.8b02725
J. Phys. Chem. Lett. 2018, 9, 6262−6268

support the redox of $Mn^{2+} \rightarrow Mn^{3+} \rightarrow Mn^{4+}$, with the magnetic moment of Mn changing from 4.51 μB in Li_2MnSiO_4 to 3.69 μB in $LiMnSiO_4$ and finally to 2.83 μB in $Li_{0.5}MnSiO_4$ (Figure 3A). In contrast, the magnetic moment of O remains nearly unchanged, indicating that the small portion of oxygen redox activity observed in the PDOS can be neglected (Figure 3A). Similar to Li_2MnSiO_4, Li_2CoSiO_4 also exhibits dominant cationic redox accompanied by a little degree of oxygen redox activity during the whole delithiation process (Figure S9). The only difference is that the oxygen redox in Li_2CoSiO_4 cannot be neglected, as indicated from Figure 3B that the magnetic moments of both O1 and O2 in Li_2CoSiO_4 increase from 0.04 to 0.26 μB from Li_2CoSiO_4 to $Li_{0.5}CoSiO_4$. While going to Li_2NiSiO_4, the redox process resembles the case of Li_2FeSiO_4 again: a Ni^{2+}/Ni^{3+} redox couple for the first Li ion extraction (per f.u.) and a polaron-like oxygen redox couple for the second Li ion extraction (Figure S10). This is also supported by the calculated magnetic moments of Ni in partially delithiated $Li_{(2-x)}NiSiO_4$ (Figure 3C), changing from 1.73 μB (Ni^{2+}, $e_g^4t_{2g}^4$) in Li_2NiSiO_4 to 2.11 μB (Ni^{3+}, $e_g^4t_{2g}^3$) in $LiNiSiO_4$ and then remaining nearly unchanged (2.11 μB for Ni in $Li_{0.5}NiSiO_4$). On the other hand, the magnetic moments of one O ion (O1) increase a little by 0.13 μB from Li_2NiSiO_4 to $LiNiSiO_4$ and then sharply change to −0.69 μB in $Li_{0.5}NiSiO_4$ (Figure 3C).

The isosurfaces of the spin density for the partially delithiated $Li_{(2-x)}TMSiO_4$ (x = 1 and 1.5) further confirm the above calculations: We observe no spin density for all of the oxygen ions in $Li_{(2-x)}MnSiO_4$, nonzero spin density for all of the oxygen ions in $Li_{(2-x)}CoSiO_4$, and large spin density with the shape of an isolated O-2p orbital on O1 in $Li_{0.5}NiSiO_4$ (Figure 3D). From the above results, we can conclude that the redox activity in $Li_{(2-x)}TMSiO_4$ (TM = Mn, Fe, Co, and Ni) shows a strong dependence on the 3d occupation numbers of the TM. This finding recalls the recent observation where a similar oxygen-polaronic effect was found in another type of polyanionic material $Li_3Fe_2(PO_4)_3$ during delithiation, while in $Li_3V_2(PO_4)_3$, the oxidation takes place on the vanadium ions.[57] A detailed discussion on the evolution of energy orbitals during delithiation explaining the above differences of the redox activity for the $Li_{(2-x)}TMSiO_4$ family is provided in Supporting Information Notes 5 and 6.

To summarize, by systematical study of the delithiation process of $Li_{(2-x)}FeSiO_4$ with the combination of first-principle calculations and sXAS measurements, we demonstrated a reversible sequent cationic and anionic redox process in $Li_{(2-x)}FeSiO_4$. Namely, the first Li ion extraction (per f.u.) is attributed to the cation valence change from Fe^{2+} to Fe^{3+}, while the second Li ion extraction activates almost exclusively the oxygen redox. This full delithiation is reversible and stable until nearly 1.8 Li ions are extracted, corresponding to an extra capacity of 0.8 Li ions induced by anionic redox activity. We then focused on slight lithiation and delithiation behaviors of $LiFeSiO_4$ from a doping perspective and demonstrated the exact transition point of cation/anion redox at $LiFeSiO_4$ (x = 1). Interestingly, both the lithiation and delithiation processes around the transition point result in electron and hole polaronic states with cationic and anionic character, respectively. In contrast to the previously reported oxygen clustering in Li-rich layered TM oxides, the oxygen polaron in $Li_{(2-x)}FeSiO_4$ is localized on a single O ion when the anion redox is triggered. Finally, the series of polyoxyanion $Li_{(2-x)}TMSiO_4$ (TM = Mn, Fe, Co, and Ni) compounds does not exhibit a universal feature of oxygen redox in general but a dependence on the 3d occupation numbers of the TM. This work provides new insights on the anionic redox activity in traditional polyanionic cathode materials and paves the way for future design of high-capacity rechargeable batteries.

■ ASSOCIATED CONTENT

Supporting Information

The Supporting Information is available free of charge on the ACS Publications website at DOI: 10.1021/acs.jpclett.8b02725.

Methods and notes on the reversibility of lithiation/delithiation for the studied compounds, the structural response to the creation of hole polarons during delithiation, sXAS results, the origin of anionic redox activity, the evolution of energy orbitals during delithiation, the average open-circuit voltage during delithiathion, and comparison of results between the hybrid functional and Lany−Zunger approach (PDF)

■ AUTHOR INFORMATION

Corresponding Authors

*E-mail: liuqh@sustc.edu.cn (Q.L.).
*E-mail: panfeng@pkusz.edu.cn (F.P.).

ORCID

Wanli Yang: 0000-0003-0666-8063
Qihang Liu: 0000-0001-9843-2482
Feng Pan: 0000-0002-8216-1339

Author Contributions

#J.Z., G.T., and J.Y. contributed equally to this work.

Notes

The authors declare no competing financial interest.

■ ACKNOWLEDGMENTS

We thank Dr. S. Lany for helpful discussions. This work was financially supported by the National Natural Science Foundation of China (No. 21603007 and 51602009), National Materials Genome Project (2016YFB0700600), and Shenzhen Science and Technology Research Grant (No. JCYJ20150729111733470 and JCYJ20151015162256516). Q.L. was supported by Guangdong Innovative and Entrepreneurial Research Team Program (Grant No. 2017ZT07C062). sXAS data were collected at beamline 8.0.1 of the Advanced Light Source, which is supported by the Director, Office of Science, Office of Basic Energy Sciences, of the U.S. Department of Energy under Contract No. DE-AC02-05CH11231.

■ REFERENCES

(1) Raebiger, H.; Lany, S.; Zunger, A. Charge Self-Regulation upon Changing the Oxidation State of Transition Metals in Insulators. *Nature* **2008**, *453*, 763.

(2) Walsh, A.; Sokol, A. A.; Buckeridge, J.; Scanlon, D. O.; Catlow, C. R. A. Oxidation States and Ionicity. *Nat. Mater.* **2018**, DOI: 10.1038/s41563-018-0165-7.

(3) Cotton, A. F.; Wilkinson, G.; Bochmann, M.; Murillo, C. A. *Advanced Inorganic Chemistry*; Wiley: New York, 1999.

(4) Wells, A. F. *Structural Inorganic Chemistry*; Oxford University Press: Oxford, U.K., 2012.

(5) Goodenough, J. B.; Kim, Y. Challenges for Rechargeable Li Batteries. *Chem. Mater.* **2010**, *22*, 587−603.

DOI: 10.1021/acs.jpclett.8b02725
J. Phys. Chem. Lett. 2018, 9, 6262−6268

(6) Lu, Z.; MacNeil, D.; Dahn, J. Layered Cathode Materials $Li[Ni_xLi_{(1/3-2x/3)}Mn_{(2/3-x/3)}]O_2$ for Lithium-Ion Batteries. *Electrochem. Solid-State Lett.* **2001**, *4*, A191−A194.
(7) Ohzuku, T.; Ueda, A.; Nagayama, M.; Iwakoshi, Y.; Komori, H. Comparative Study of $LiCoO_2$, $LiNi_{12}Co_{12}O_2$ and $LiNiO_2$ for 4 V Secondary Lithium Cells. *Electrochim. Acta* **1993**, *38*, 1159−1167.
(8) Ren, H.; Huang, Y.; Wang, Y.; Li, Z.; Cai, P.; Peng, Z.; Zhou, Y. Effects of Different Carbonate Precipitators on $LiNi_{1/3}Co_{1/3}Mn_{1/3}O_2$ Morphology and Electrochemical Performance. *Mater. Chem. Phys.* **2009**, *117*, 41−45.
(9) Mizushima, K.; Jones, P.; Wiseman, P.; Goodenough, J. B. Li_xCoO_2 ($0< x<-1$): A New Cathode Material for Batteries of High Energy Density. *Mater. Res. Bull.* **1980**, *15*, 783−789.
(10) Sathiya, M.; Rousse, G.; Ramesha, K.; Laisa, C.; Vezin, H.; Sougrati, M. T.; Doublet, M.; Foix, D.; Gonbeau, D.; Walker, W.; et al. Reversible Anionic Redox Chemistry in High-Capacity Layered-Oxide Electrodes. *Nat. Mater.* **2013**, *12*, 827.
(11) McCalla, E.; Abakumov, A. M.; Saubanère, M.; Foix, D.; Berg, E. J.; Rousse, G.; Doublet, M.-L.; Gonbeau, D.; Novák, P.; Van Tendeloo, G.; et al. Visualization of OO Peroxo-Like Dimers in High-Capacity Layered Oxides for Li-Ion Batteries. *Science* **2015**, *350*, 1516−1521.
(12) McCalla, E.; Sougrati, M. T.; Rousse, G.; Berg, E. J.; Abakumov, A.; Recham, N.; Ramesha, K.; Sathiya, M.; Dominko, R.; Van Tendeloo, G.; et al. Understanding the Roles of Anionic Redox and Oxygen Release During Electrochemical Cycling of Lithium-Rich Layered Li_4FeSbO_6. *J. Am. Chem. Soc.* **2015**, *137*, 4804−4814.
(13) Sathiya, M.; Leriche, J.-B.; Salager, E.; Gourier, D.; Tarascon, J.-M.; Vezin, H. Electron Paramagnetic Resonance Imaging for Real-Time Monitoring of Li-Ion Batteries. *Nat. Commun.* **2015**, *6*, 6276.
(14) Grimaud, A.; Hong, W.; Shao-Horn, Y.; Tarascon, J.-M. Anionic Redox Processes for Electrochemical Devices. *Nat. Mater.* **2016**, *15*, 121−126.
(15) Luo, K.; Roberts, M. R.; Guerrini, N.; Tapia-Ruiz, N.; Hao, R.; Massel, F.; Pickup, D. M.; Ramos, S.; Liu, Y.-S.; Guo, J.; et al. Anion Redox Chemistry in the Cobalt Free 3d Transition Metal Oxide Intercalation Electrode $Li[Li_{0.2}Ni_{0.2}Mn_{0.6}]O_2$. *J. Am. Chem. Soc.* **2016**, *138*, 11211−11218.
(16) Seo, D.-H.; Lee, J.; Urban, A.; Malik, R.; Kang, S.; Ceder, G. The Structural and Chemical Origin of the Oxygen Redox Activity in Layered and Cation-Disordered Li-Excess Cathode Materials. *Nat. Chem.* **2016**, *8*, 692−697.
(17) Pearce, P. E.; Perez, A. J.; Rousse, G.; Saubanère, M.; Batuk, D.; Foix, D.; McCalla, E.; Abakumov, A. M.; Van Tendeloo, G.; Doublet, M.-L.; et al. Evidence for Anionic Redox Activity in a Tridimensional-Ordered Li-Rich Positive Electrode β-Li_2IrO_3. *Nat. Mater.* **2017**, *16*, 580−586.
(18) Saubanère, M.; McCalla, E.; Tarascon, J.-M.; Doublet, M.-L. The Intriguing Question of Anionic Redox in High-Energy Density Cathodes for Li-Ion Batteries. *Energy Environ. Sci.* **2016**, *9*, 984−991.
(19) Xie, Y.; Saubanère, M.; Doublet, M.-L. Requirements for Reversible Extra-Capacity in Li-Rich Layered Oxides for Li-Ion Batteries. *Energy Environ. Sci.* **2017**, *10*, 266−274.
(20) Lu, N.; Zhang, P.; Zhang, Q.; Qiao, R.; He, Q.; Li, H.-B.; Wang, Y.; Guo, J.; Zhang, D.; Duan, Z.; et al. Electric-Field Control of Tri-State Phase Transformation with a Selective Dual-Ion Switch. *Nature* **2017**, *546*, 124.
(21) Freire, M.; Kosova, N.; Jordy, C.; Chateigner, D.; Lebedev, O.; Maignan, A.; Pralong, V. A New Active Li-Mn-O Compound for High Energy Density Li-Ion Batteries. *Nat. Mater.* **2016**, *15*, 173−177.
(22) Fang, C.; Huang, Y.; Yuan, L.; Liu, Y.; Chen, W.; Huang, Y.; Chen, K.; Han, J.; Liu, Q.; Huang, Y. A Metal−Organic Compound as Cathode Material with Superhigh Capacity Achieved by Reversible Cationic and Anionic Redox Chemistry for High-Energy Sodium-Ion Batteries. *Angew. Chem.* **2017**, *129*, 6897−6901.
(23) Jung, S.-K.; Kang, K. Simultaneous Anionic and Cationic Redox. *Nat. Energy* **2017**, *2*, 912.
(24) Li, B.; Xia, D. Anionic Redox in Rechargeable Lithium Batteries. *Adv. Mater.* **2017**, *29*, 1701054.
(25) Perez, A. J.; Jacquet, Q.; Batuk, D.; Iadecola, A.; Saubanère, M.; Rousse, G.; Larcher, D.; Vezin, H.; Doublet, M.-L.; Tarascon, J.-M. Approaching the Limits of Cationic and Anionic Electrochemical Activity with the Li-Rich Layered Rocksalt Li_3IrO_4. *Nat. Energy* **2017**, *2*, 954.
(26) Lee, E.; Persson, K. A. Structural and Chemical Evolution of the Layered Li-Excess Li_xMnO_3 as a Function of Li Content from First-Principles Calculations. *Adv. Energy Mater.* **2014**, *4*, 1400498.
(27) Koga, H.; Croguennec, L.; Ménétrier, M.; Douhil, K.; Belin, S.; Bourgeois, L.; Suard, E.; Weill, F.; Delmas, C. Reversible Oxygen Participation to the Redox Processes Revealed for $Li_{1.20}Mn_{0.54}Co_{0.13}Ni_{0.13}O_2$. *J. Electrochem. Soc.* **2013**, *160*, A786−A792.
(28) Oishi, M.; Yogi, C.; Watanabe, I.; Ohta, T.; Orikasa, Y.; Uchimoto, Y.; Ogumi, Z. Direct Observation of Reversible Charge Compensation by Oxygen Ion in Li-Rich Manganese Layered Oxide Positive Electrode Material, $Li_{1.16}Ni_{0.15}Co_{0.19}Mn_{0.50}O_2$. *J. Power Sources* **2015**, *276*, 89−94.
(29) Chen, H.; Islam, M. S. Lithium Extraction Mechanism in Li-Rich Li_2MnO_3 Involving Oxygen Hole Formation and Dimerization. *Chem. Mater.* **2016**, *28*, 6656−6663.
(30) Xiao, R.; Li, H.; Chen, L. Density Functional Investigation on Li_2MnO_3. *Chem. Mater.* **2012**, *24*, 4242−4251.
(31) Oishi, M.; Yamanaka, K.; Watanabe, I.; Shimoda, K.; Matsunaga, T.; Arai, H.; Ukyo, Y.; Uchimoto, Y.; Ogumi, Z.; Ohta, T. Direct Observation of Reversible Oxygen anion Redox Reaction in Li-Rich Manganese Oxide, Li_2MnO_3, Studied by Soft X-ray Absorption Spectroscopy. *J. Mater. Chem. A* **2016**, *4*, 9293−9302.
(32) Wu, S. Q.; Zhu, Z. Z.; Yang, Y.; Hou, Z. F. Structural Stabilities, Electronic Structures and Lithium Deintercalation in Li_xMSiO_4 (M = Mn, Fe, Co, Ni): A GGA and GGA+U Study. *Comput. Mater. Sci.* **2009**, *44*, 1243−1251.
(33) Zhang, P.; Hu, C.; Wu, S.; Zhu, Z.; Yang, Y. Structural Properties and Energetics of Li_2FeSiO_4 Polymorphs and Their Delithiated Products from First-Principles. *Phys. Chem. Chem. Phys.* **2012**, *14*, 7346−7351.
(34) Yang, J.; Kang, X.; He, D.; Zheng, A.; Pan, M.; Mu, S. Graphene Activated 3D-Hierarchical Flower-like Li_2FeSiO_4 for High-Performance Lithium-Ion Batteries. *J. Mater. Chem. A* **2015**, *3*, 16567−16573.
(35) Wu, X.; Jiang, X.; Huo, Q.; Zhang, Y. Facile Synthesis of Li_2FeSiO_4/C Composites with Triblock Copolymer P123 and Their Application as Cathode Materials for Lithium Ion Batteries. *Electrochim. Acta* **2012**, *80*, 50−55.
(36) Kamon-in, O.; Buakeaw, S.; Klysubun, W.; Limphirat, W.; Srilomsak, S.; Meethong, N. A Study of Transient Phase Transformation in LFS/C using in-Situ Time Resolved X-Ray Absorption Spectroscopy. *Int. J. Electrochem. Sci.* **2014**, *9*, 4257−4267.
(37) Lv, D.; Wen, W.; Huang, X.; Bai, J.; Mi, J.; Wu, S.; Yang, Y. A Novel Li_2FeSiO_4/C Composite: Synthesis, Characterization and High Storage Capacity. *J. Mater. Chem.* **2011**, *21*, 9506−9512.
(38) Zhao, Y.; Li, J.; Wang, N.; Wu, C.; Ding, Y.; Guan, L. In Situ Generation of Li_2FeSiO_4 Coating on MWNT as a High Rate Cathode Material for Lithium Ion Batteries. *J. Mater. Chem.* **2012**, *22*, 18797−18800.
(39) Masese, T.; Tassel, C.; Orikasa, Y.; Koyama, Y.; Arai, H.; Hayashi, N.; Kim, J.; Mori, T.; Yamamoto, K.; Kobayashi, Y.; et al. Crystal Structural Changes and Charge Compensation Mechanism during Two Lithium Extraction/Insertion between Li_2FeSiO_4 and $FeSiO_4$. *J. Phys. Chem. C* **2015**, *119*, 10206−10211.
(40) Li, Y.; Cheng, X.; Zhang, Y. Achieving High Capacity by Vanadium Substitution into Li_2FeSiO_4. *J. Electrochem. Soc.* **2011**, *159*, A69−A74.
(41) Kokalj, A.; Dominko, R.; Mali, G.; Meden, A.; Gaberscek, M.; Jamnik, J. Beyond One-Electron Reaction in Li Cathode Materials: Designing $Li_2Mn_xFe_{1-x}SiO_4$. *Chem. Mater.* **2007**, *19*, 3633−3640.
(42) Yang, J. L.; Zheng, J. X.; Kang, X. C.; Teng, G. F.; Hu, L.; Tan, R.; Wang, K.; Song, X. H.; Xu, M.; Mu, S. C.; et al. Tuning Structural Stability and Lithium-Storage Properties by d-Orbital Hybridization

DOI: 10.1021/acs.jpclett.8b02725
J. Phys. Chem. Lett. 2018, 9, 6262−6268

Substitution in Full Tetrahedron Li_2FeSiO_4 Nanocrystal. *Nano Energy* **2016**, *20*, 117−125.
(43) Heyd, J.; Scuseria, G. E.; Ernzerhof, M. Hybrid Functionals based on a Screened Coulomb Potential. *J. Chem. Phys.* **2003**, *118*, 8207−8215.
(44) Nishimura, S.-i.; Hayase, S.; Kanno, R.; Yashima, M.; Nakayama, N.; Yamada, A. Structure of Li_2FeSiO_4. *J. Am. Chem. Soc.* **2008**, *130*, 13212−13213.
(45) Pacchioni, G.; Frigoli, F.; Ricci, D.; Weil, J. A. Theoretical Description of Hole Localization in a Quartz Al Center: The Importance of Exact Electron Exchange. *Phys. Rev. B: Condens. Matter Mater. Phys.* **2000**, *63*, 054102.
(46) Chan, J. A.; Lany, S.; Zunger, A. Electronic Correlation in Anion *p* Orbitals Impedes Ferromagnetism due to Cation Vacancies in Zn Chalcogenides. *Phys. Rev. Lett.* **2009**, *103*, 016404.
(47) Lægsgaard, J.; Stokbro, K. Hole Trapping at Al Impurities in Silica: a Challenge for Density Functional Theories. *Phys. Rev. Lett.* **2001**, *86*, 2834−2837.
(48) Mori-Sánchez, P.; Cohen, A. J.; Yang, W. Localization and Delocalization Errors in Density Functional Theory and Implications for Band-Gap Prediction. *Phys. Rev. Lett.* **2008**, *100*, 146401.
(49) Lany, S.; Zunger, A. Polaronic Hole Localization and Multiple Hole Binding of Acceptors in Oxide Wide-Gap Semiconductors. *Phys. Rev. B: Condens. Matter Mater. Phys.* **2009**, *80*, 085202.
(50) Lany, S.; Raebiger, H.; Zunger, A. Magnetic Interactions of Cr-Cr and Co-Co Impurity Pairs in ZnO within a Band-Gap Corrected Density Functional Approach. *Phys. Rev. B: Condens. Matter Mater. Phys.* **2008**, *77*, 241201.
(51) Peng, H.; Lany, S. Semiconducting Transition-Metal Oxides Based on d5 Cations: Theory for MnO and Fe_2O_3. *Phys. Rev. B: Condens. Matter Mater. Phys.* **2012**, *85*, 201202.
(52) Lyness, C.; Delobel, B.; Armstrong, A. R.; Bruce, P. G. The Lithium Intercalation Compound Li_2CoSiO_4 and its Behaviour as a Positive Electrode for Lithium Batteries. *Chem. Commun.* **2007**, 4890−4892.
(53) Armstrong, A. R.; Lyness, C.; Ménétrier, M.; Bruce, P. G. Structural Polymorphism in Li_2CoSiO_4 Intercalation Electrodes: a Combined Diffraction and NMR Study. *Chem. Mater.* **2010**, *22*, 1892−1900.
(54) Gong, Z.; Li, Y.; Yang, Y. Synthesis and Electrochemical Performance of Li_2CoSiO_4 as Cathode Material for Lithium Ion Batteries. *J. Power Sources* **2007**, *174*, 524−527.
(55) Gummow, R.; He, Y. Recent Progress in the Development of Li_2MnSiO_4 Cathode Materials. *J. Power Sources* **2014**, *253*, 315−331.
(56) Yang, X.-F.; Yang, J.-H.; Zaghib, K.; Trudeau, M. L.; Ying, J. Y. Synthesis of Phase-Pure Li_2MnSiO_4@ C Porous Nanoboxes for High-Capacity Li-Ion Battery Cathodes. *Nano Energy* **2015**, *12*, 305−313.
(57) Younesi, R.; Christiansen, A.; Loftager, S.; García-Lastra, J. M.; Vegge, T.; Norby, P.; Holtappels, P. Charge Localization in the Lithium Iron Phosphate $Li_3Fe_2(PO_4)_3$ at High Voltages in Lithium-Ion Batteries. *ChemSusChem* **2015**, *8*, 3213−3216.

DOI: 10.1021/acs.jpclett.8b02725
J. Phys. Chem. Lett. 2018, 9, 6262−6268